Magneto-optical relaxation measurements for the characterization of biomolecular interactions



2006 J. Phys.: Condens. Matter 18 S2847

(http://iopscience.iop.org/0953-8984/18/38/S21)

INSTITUTE OF PHYSICS PUBLISHING JOURNAL OF PHYSICS: CONDENSED MATTER

J. Phys.: Condens. Matter **18** (2006) S2847–S2863 doi:10.1088/0953-8984/18/38/S21

# Magneto-optical relaxation measurements for the characterization of biomolecular interactions

**K Aurich**[1], **G Glöckl**[1], **E Romanus**[2], **P Weber**[3], **S Nagel**[1] **and W Weitschies**[1]

[1] Institute of Pharmacy, Ernst-Moritz-Arndt-University Greifswald, 17487 Greifswald, Germany
[2] Federal Institute for Occupational Safety and Health, 44149 Dortmund, Germany
[3] Institute of Solid State Physics, Friedrich-Schiller-University Jena, 07743 Jena, Germany

E-mail: werner.weitschies@uni-greifswald.de

Received 1 May 2006, in final form 4 July 2006
Published 8 September 2006
Online at stacks.iop.org/JPhysCM/18/S2847

**Abstract**

Measurements of the magneto-optical relaxation of ferrofluids (MORFF) were applied as a novel homogeneous immunoassay for the investigation of biomolecular interactions. The technique is based on magnetic nanoparticles (MNP) functionalized with antibodies. The relaxation time of the optical birefringence that occurs when a pulsed magnetic field is applied to the nanoparticle suspension depends on the particle size. This enables the detection of particle aggregates formed after the addition of the antigen coupling partner. MORFF size measurements on the original ferrofluid and its fractions obtained by magnetic fractionation are comparable with results from other methods such as atomic force microscopy and photon correlation spectroscopy. In kinetic studies, the binding properties of five antigens and their polyclonal antibodies were investigated: human immunoglobulin G (hIgG), human immunoglobulin M (hIgM), human Eotaxin (hEotaxin), human carcinoembryonic antigen (hCEA), and human insulin (hInsulin). The enlargement of the relaxation time observed during the coupling experiments is expressed in terms of a size distribution function, which includes MNP monomers as well as aggregates. The kinetic process can be described by a model of stepwise polymerization. The kinetic parameters obtained are compared to results of surface plasmon resonance measurements.

## 1. Introduction

Magnetic nanoparticles (MNP) offer some attractive possibilities for the determination of biomolecular interactions. The nanoparticles can be coated with biological molecules in order to generate an interaction with a biological entity of interest. Moreover, due to their magnetic properties the nanoparticles can be manipulated by an external magnetic field [1]. Established

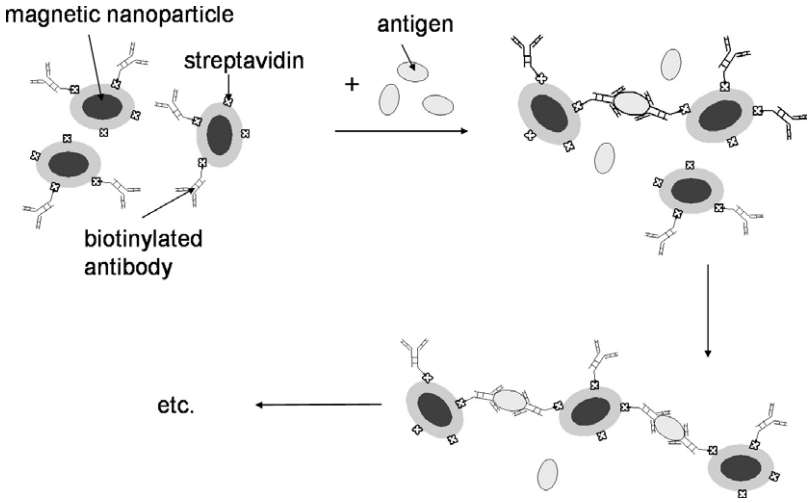


**Figure 1.** Scheme of formation of aggregates due to the binding reaction between antibody–MNP and antigen.

techniques such as magnetic cell separation use magnetic field gradients to separate magnetic labelled cells [2]. More recently, magnetic immunoassay techniques have been developed in which the magnetic field generated by the magnetic labelled targets is directly detected with a sensitive magnetometer [3, 4]. The measurement of the magneto-optical relaxation of ferrofluids takes advantage of the ability of MNP to influence optical properties in liquids in the presence of a magnetic field. Utilizing this effect, measurements of the magneto-optical relaxation of ferrofluids (MORFF) can be applied as a novel tool for the determination of binding reactions and appropriate kinetics, between biomolecules in a liquid phase, without any additional signal generators.

A ferrofluid is a colloidal suspension of MNP. In order to prevent aggregation due to Van der Waals and magnetic interactions, the particles are coated with shell materials [5]. A primary isotropic ferrofluid with freely movable MNP can be forced into an anisotropic state of order by an external magnetic field yielding the magnetic moments of the individual particles to align along the field direction. Thereby an optical birefringence is induced, that is also referred to as the Cotton–Mouton effect [6]. Switching off the magnetic field, a decay of the magnetization occurs due to the particles' Brownian rotational diffusion associated with the relaxation of the birefringence. Since the Brownian relaxation markedly depends on the particles' hydrodynamic diameter particle size measurements are feasible. For a more comprehensive characterization of the ferrofluid additional size measurements by light scattering measurements and AFM are arranged.

Further on, biomolecular binding events are detectable using labelled MNP due to the increase of the hydrodynamic diameter in consequence of the formation of aggregates during the interaction. Whereas binding of single molecules to the particles generates rather small increases of the effective particle sizes, cross-linking of MNP via coupling partners (figure 1) yields more pronounced effects on the relaxation behaviour. This offers the opportunity to determine kinetic parameters of the underlying processes, i.e. the affinity of binding partners such as antigen and antibody.

We investigated five polyclonal antibody/antigen systems by MORFF. At first, as model systems with different structures antibodies against human immunoglobulin G (hIgG) as well as

human immunoglobulin M (hIgM) were coupled with the MNP. Furthermore, clinical relevant systems were chosen. Human Eotaxin (hEotaxin) is a CC chemokine with a molecular weight of 8.4 kDa. Chemokines are small secreted proteins that are critically involved in many biological processes, including immune surveillance, inflammation and development. Due to its preferential, powerful action on eosinophils and its occurrence in different species, hEotaxin is considered the most relevant chemokine in the pathophysiology of allergic conditions and asthma [7–9]. Furthermore, the interaction between human CEA (hCEA; 180 kDa) and its antibody was analysed. hCEA is an oncofoetal antigen, which is only detectable on tumours and the luminal surface of the gut. It is highly expressed in most gastrointestinal carcinomas and in a number of breast, lung and ovarian carcinomas [10].

For more than 40 years the concentration of hInsulin (hInsulin; 5.8 kDa) in blood samples has been estimated immunochemically. The introduction of radioimmunoassay (RIA) provided a method for measuring hInsulin in plasma and serum [11]. RIA and later developed enzyme immunoassays [12] for detecting hInsulin require additional steps for labelling the anti-hInsulin antibody with either radioactive or enzyme markers. The detection of hInsulin by homogeneous immunoassays facilitates the performance without any markers.

The obtained kinetic behaviour of the clinically relevant antigen/antibody systems is compared with data derived from surface plasmon resonance (SPR) analyses with the identical systems. The SPR method is a label free technology for monitoring biomolecular interactions. Thereby, one of the binding partners (the ligand, in this case the antibody) is immobilized onto the sensor chip surface; the other (the analyte, the antigen) is free in solution and passes over the surface. Association and dissociation are measured instantly in so-called response units. The SPR technique is an immunological biosensor method, and allows signal generation between antibody and antigen in real time. Although the SPR method differs from the here presented method, SPR is chosen as an established reference method due to its ability to determine kinetic parameters of antigen antibody systems.

## 2. Material and methods

### *2.1. Magnetic nanoparticles and fractionation*

The magnetic nanoparticles utilized for our studies (DDM 128N, Meito Sangyo, Japan) consist of ferrimagnetic cores of maghemite coated with carboxydextran shells. The coating is due to reduction of magnetic dipole–dipole interactions as well as aggregation phenomena. The particles are suspended in water forming a stable dark brown dispersion referred to as ferrofluid. Meanwhile the particle size distribution is well characterized as described in detail by Büscher *et al* [5]. In short, particle core sizes of the original solution and size-fractionated samples (see below) were examined by means of atomic force microscopy (AFM) resulting in a log-normal size distribution with core diameters in the range of 6–40 nm. Evidence suggests larger cores to be composed of aggregates of single particles not larger than 20 nm in diameter surrounded by a multitude of small ones. When comparing AFM with light scattering experiments the cores appear to be coated with uniform shells the thickness of which is dependent on the swelling state (2–4 nm). The particles are well stabilized by ionic repulsion. We determined a zeta potential of −40 mV.

The fractionation of magnetic nanosized particles was accomplished using the principle of magnetic cell separation. Attractive forces by virtue of inhomogeneous magnetic fields generated by a magnetic separation column (MACS® LS, Miltenyi Biotech, Bergisch Gladbach, Germany) within a tunable electromagnetic field (Bruker, Karlsruhe, Germany) result in retention of particles within the column depending on the particle magnetic moment, i.e.

**Table 1.** Antibodies used for coupling with the streptavidin MNP.

| Antibody species | Host | Amount | Supplier |
|---|---|---|---|
| hIgG | Mouse | 1 nmol | Jackson IR Lab. Inc., West Grove, PA, USA |
| hIgM | Goat | 1 nmol | Jackson IR Lab. Inc., West Grove, PA, USA |
| hEotaxin | Rabbit | 0.33 nmol | Serotec, UK |
| hInsulin | Chicken | 0.33 nmol | GenWay Biotech Inc., USA |
| hCEA | Chicken | 0.33 nmol | USBiological, USA |

particle core volume. The lower the magnetic field strength the larger the particles just adhering to the column.

For reducing the amount of small particles exhibiting no or only a slight birefringence signal, a fractionation was performed prior to biological functionalization. Therefore, a separation column (Miltenyi MACS® LS) was placed in a permanent magnetic field of about 100 mT generated by two opposing Nd–Fe–B magnets. The column was rinsed with water three times. Then 500 $\mu$l of the original ferrofluid were added and then there was rinsing with water until the eluate became uncoloured. Subsequently, the column was removed from the magnets and retained particles were eluted with water.

### *2.2. Functionalization*

Streptavidin was coupled with MNP via the periodate method as previously described [13]. For the preparation of antibody coupled MNP five biotinylated polyclonal antibodies of different amounts were chosen. During the development of the method the required antibody amount for 500 $\mu$l streptavidin–MNP could be decreased from 1 nmol at the beginning down to 0.33 nmol at present. The antibody was combined with the streptavidin–MNP utilizing the streptavidin–biotin binding system. For this purpose, 500 $\mu$l streptavidin–MNP were incubated with the adequate amount of the previously biotinylated antibody for 2 h at 4 °C in 6 ml phosphate buffered saline (PBS; 120 mM NaCl, 2.7 mM KCl in phosphate buffer 10 mM, pH 7.4). In order to saturate remaining binding sites 0.4 $\mu$mol biotin were added followed by purification via magnetic separation. The antibody coupled particles were stable for nearly four weeks in 0.1% bovine serum albumin (BSA; Sigma Aldrich, Germany) and 0.02% $NaN_3$ in PBS. Table 1 shows the antibodies coupled with MNP.

### *2.3. Magneto-optical relaxation device*

In the presence of magnetic fields, suspended and freely movable magnetic particles preferentially align in the direction of the external field inducing an optical anisotropy, i.e. a birefringence, into the suspension. This effect is mainly due to the particles shape anisotropy, other anisotropies like magnetocrystalline or surface anisotropy are considered to play a subordinate role for the investigated ferrofluid [14].

When switching off the magnetizing field the particles favoured direction relaxes in the course of time until statistical orientation resulting in a total collapse of the birefringence $\Delta n$. Assuming monodisperse MNP the decay accords to [15]:

$$\Delta n = \Delta n_0 \mathrm{e}^{-\frac{t}{\tau}} \tag{1}$$

with $\Delta n_0$ being the initial birefringence. This decay is mainly affected by the hydrodynamic particle volume $V_{\mathrm{hyd}}$ applying the well-known Brown equation [15]:

$$\tau_{\mathrm{B}} = \frac{3\eta V_{\mathrm{hyd}}}{kT} \tag{2}$$

with $\eta$ being the viscosity and $kT$ the thermal energy.

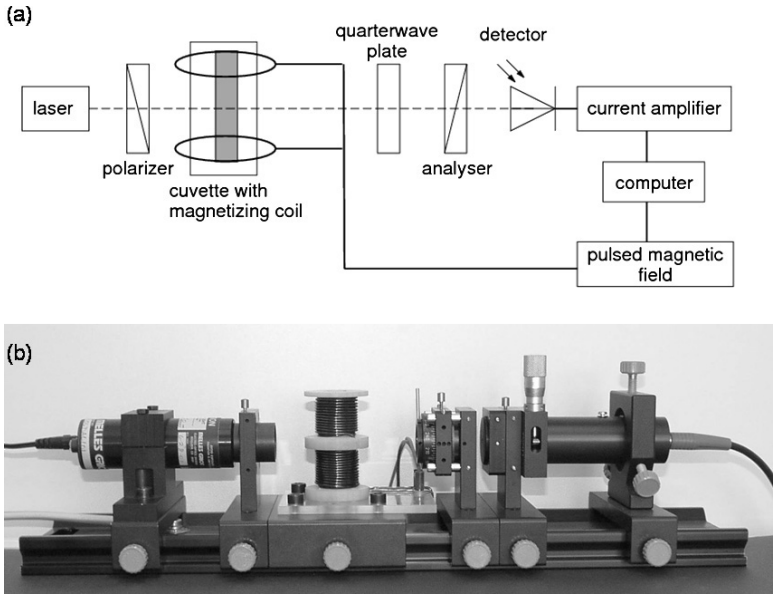


**Figure 2.** (a) MORFF measurement set-up (schematic); (b) optical bench.

Exploiting this phenomenon a magneto-optical relaxation device described in detail by Romanus *et al* [16] was established. In short, the measurement set-up consists of an optical bench with aligned laser, polarizer, magnetizing coil containing the sample cuvette, analyser, retardation plate and photodiode detector (figure 2). The polarizer and analyser are directed perpendicular to each other and at 45° to the magnetizing field. The slow axis of the retardation plate is oriented nearly parallel to the polarizer. A low noise current amplifier intensifies the photocurrent of the photodiode detector. The phase shift $\varphi$ of the birefringence is given by [17]

$$\varphi = \frac{2\pi}{\lambda} d_s \Delta n, \tag{3}$$

where $d_s$ is the thickness of the sample and $\lambda$ is the wavelength of the laser light. For the relatively weak concentrations of the ferrofluid, and the retardation plate being slightly out of tune, the light flux $I$ impinging on the detector is proportional to $\varphi$. Accordingly, the measured signal after switching off the magnetizing field can be analysed when fitting to the equation:

$$I(t) = I_0 \mathrm{e}^{-\frac{t}{\tau_B}}. \tag{4}$$

Over the past few years the device has been continuously improved. The final design is as follows: a pulsed magnetic field of up to 10 kA m$^{-1}$ with adjustable magnetizing time in the range of 1–500 ms is applied to the sample while continuously recording the optical signal impinging on the detector. The entire system is controlled by a PC running LabVIEW®. A 20 MHz I/O board collects and processes the data and controls the measurement equipment. The user is allowed to execute a series of measurements in order to follow up binding reactions of functionalized MNP over a predefined period.

For the measurements presented here, an asymmetrically pulsed magnetic field of 10 Hz (20 ms magnetizing time) and 5.4 kA m$^{-1}$ was applied to the samples. Experiments were performed in glass cuvettes (J 103, Hellma, Germany) at room temperature.

### *2.4. Data analysis*

The exponential fit (4) describes the relaxation behaviour of monodisperse particles. For a particle system with a broad size distribution $P(d_{\mathrm{hyd}})$, the superposition of signals of MNP with different relaxation times results as

$$I(t) = \int I_0(d_{\mathrm{hyd}}) \exp[-t/\tau(d_{\mathrm{hyd}})] \cdot P(d_{\mathrm{hyd}})\, \mathrm{d}d_{\mathrm{hyd}}. \tag{5}$$

In our model, we neglect the dependence of the static birefringence $I_0$ on the particle hydrodynamic diameter $d_{\mathrm{hyd}}$ of the single particles. Taking the log-normal distribution with its density function

$$P(d) = \frac{1}{\sqrt{2\pi}\sigma_L}\frac{1}{d}\exp\left[-\frac{(\ln d - \ln \mu_L)^2}{2\sigma_L^2}\right], \tag{6}$$

the signal is determined by the parameters $\mu_{\mathrm{L}}$ and $\sigma_{\mathrm{L}}$. The expression (5) with function (6) was solved numerically, and the distribution parameters were fitted to experimental relaxation data using numerical integration and nonlinear fit routines of Mathematica®.

Changes of the particle sizes during ongoing reaction reflect the coupling processes between functionalized MNP and antigen molecules. Whereas the small size effect of single antigen molecules bound at particles is neglected in our consideration, cross-linking of MNP via coupling partners can be expressed in terms of the partition function. To benefit from standard methods for the statistical description of stepwise polymerization, we assume the formation of linear chains according to the reaction scheme

$$n\ \mathrm{A\text{–}A} + n\ \mathrm{B\text{–}B} \rightarrow \mathrm{B\text{–}B\text{–}[\text{–}A\text{–}A\text{–}B\text{–}B\text{–}]}_{n-1}\text{–}\mathrm{A\text{–}A}.$$

Here, two antibodies B linked to the same MNP are symbolized by B–B, whereas A–A denotes the antigen molecule with two binding sites (epitopes) A. To ensure a constant static birefringence $I_0$ during the coupling reaction, we assume the contribution of an $n$-mer to the total birefringence to be proportional to $n$.

Proceeding from results for the step polymerization of $A_2$ and $B_2$ molecules (see e.g. [18]), the calculation of the total number of particles bound in MNP chains of the length $n$ is straightforward. We obtained the expression

$$P_n(\alpha) = n(1-\alpha)^2\alpha^{n-1}, \qquad \alpha = rp^2, \tag{7}$$

where $r$ is the stoichiometric ratio of binding sites at the reaction start defined as

$$r = \frac{c_{\mathrm{A},0}}{c_{\mathrm{B},0}}, \tag{8}$$

and $p$ is the conversion

$$p(t) = \frac{c_{\mathrm{A},0} - c_{\mathrm{A}}(t)}{c_{\mathrm{A},0}} \tag{9}$$

of binding site A which is the limiting reagent in our considerations ($r \leqslant 1$). For the case of monodisperse monomers, the total distribution function results from a summation of the particle numbers as

$$P(d) = \sum_{n=1}^{\infty} P_n \delta(d - d_n). \tag{10}$$

By integration of the delta distribution $\delta(d)$ we obtained for the signal function

$$I(t) = I_0(1-\alpha)^2 \sum_{n=1}^{\infty} n\alpha^{n-1} \exp[-t/\tau_n], \tag{11}$$

where $\tau_n$ is the relaxation time of an $n$-mer. A more realistic description has to include the broad distribution function of monomers. For sake of simplicity, instead of the slightly unsymmetrical log-normal distribution resulting from the fit of the relaxation signal of unbound MNP, the monomers are described by the Gaussian distribution

$$P(d) = \frac{1}{\sqrt{2\pi}\sigma} \exp\left[-\frac{(d-\mu)^2}{2\sigma^2}\right]. \tag{12}$$

For the mean and the standard deviation of a $n$-mer distribution we take the approximation

$$\mu_n = n\mu, \qquad \sigma_n = \sqrt{n}\sigma. \tag{13}$$

Inserting the result for the total distribution function

$$P(d) = \sum_{n=1}^{\infty} P_n(\alpha) \frac{1}{\sqrt{2\pi}\sigma_n} \exp\left[-\frac{(d-\mu_n)^2}{2\sigma_n^2}\right] \tag{14}$$

into equation (5), the relaxation signal $I(t)$ is expressed in terms of the parameters of the initial distribution function $\mu$ and $\sigma$ and of the polymerization degree. For the analysis of relaxation data, we fitted the parameters of the Gaussian distribution to the relaxation signal of the MNP suspension obtained before the addition of antigen. This suspension is assumed to consist only of monomers. The relaxation signals measured after starting the coupling reaction by adding antigen were fitted using the distribution function (14) with fixed parameters $\mu$ an $\sigma$. As the only variable parameter we used $\alpha$, which determines the degree of polymerization. $\alpha$ was obtained using numerical integration and nonlinear fit routines of Mathematica®.

The time dependence of the resulting polymerization degree can be compared with kinetic calculations, which consider the elementary binding process between antigen and antibody. The conversion of binding sites A (antigen epitopes) and B (antibodies) in the reaction

$$\mathrm{A} + \mathrm{B} \underset{k_d}{\overset{k_a}{\rightleftarrows}} \mathrm{AB} \tag{15}$$

is determined by the kinetic equation

$$\frac{\mathrm{d}c_\mathrm{A}}{\mathrm{d}t} = -\frac{1}{c_{\mathrm{A},0}} \frac{\mathrm{d}p}{\mathrm{d}t} = -k_a c_\mathrm{A} c_\mathrm{B} + k_d c_\mathrm{AB}. \tag{16}$$

This differential equation was solved numerically, and the kinetic parameters $k_a$ and $k_d$ were optimized with respect to the conversions calculated from the experimental relaxation signal.

### *2.5. Surface plasmon resonance (SPR)*

In order to compare the kinetic behaviour obtained by MORFF an investigation of the reaction kinetics of hEotaxin, hCEA, and hInsulin and their polyclonal antibodies was performed with the SPR method. The BIAcore X instrument as well as the CM5 sensor chips, the HBS-EP buffer (10 mM HEPES/150 mM NaCl/3 mM EDTA/0.005% polysorbate 20) pH 7.5, the amine coupling kit containing $N$-hydroxysuccinimide (NHS), $N$-ethyl-$N'$-(3-dimethyl-aminopropyl)-carbodiimide (EDC), and ethanolamine–HCl were purchased from BIAcore International AB, Sweden. All experiments were performed twice, at 25 ± 0.1 °C and with HBS-EP as the buffer solution.

Immobilization of the antibodies onto the BIAcore sensor chip by the amine coupling method was executed as described elsewhere [19]. In order to determine unspecific bonds the second flow cell was prepared with polyclonal IgG from goats. For binding experiments

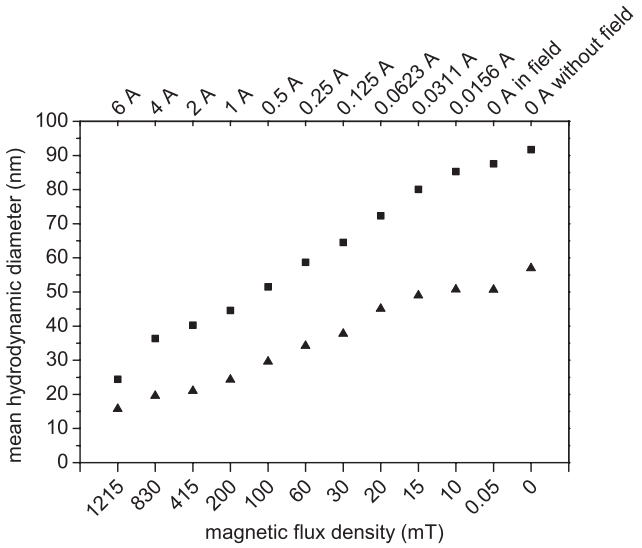


**Figure 3.** Hydrodynamic diameters of different fractions obtained by magnetic fractionation of the original ferrofluid. The fraction numbers are assigned to the currents yielding the magnetizing forces used for the magnetic fractionation. Results from MORFF (triangles) are compared with PCS measurements (squares).

the antigen solution was injected into the flow cell at a flow rate of 30 $\mu$l min$^{-1}$ (hEotaxin), 40 $\mu$l min$^{-1}$ (hCEA) or 60 $\mu$l min$^{-1}$ (hInsulin), respectively, to allow an association phase. The cell was then filled with running buffer for the dissociation phase. The antibody could be regenerated in any case by a regeneration solution according to Andersson *et al* [20].

The SPR response prior to injection and the time of injection were adjusted to zero. Binding curves were corrected for changes in the refractive angle of the buffer and non-specific bonds in the reference cell by means of the BIAcore Control software. Corrected binding curves of the antigen association and dissociation were quantitatively analysed using BIAcore Evaluation Software. Data were fitted to a simple 1:1 (Langmuir) binding model ($A + B \leftrightarrow AB$).

## 3. Results

### *3.1. Particle size measurement/size distribution analysis*

The suspension of magnetic nanoparticles was characterized by magnetic fractionation, and the magneto-optical relaxation signals of the individual fractions were analysed utilizing the exponential function (4). Hydrodynamic diameters obtained from MORFF are compared with PCS measurements in figure 3. With both methods, a systematic increase of diameter with decreasing magnetic field strength used for the fractionation was found. For all fractions, the particle sizes measured by MORFF are smaller by a factor of about 0.6.

As shown in figure 4, the signal relaxation of the 0.5 A ferrofluid fraction cannot be described properly by an exponential decay. Utilizing equation (5) with optimized parameters of the log-normal distribution (6) $\sigma_L = 0.39$ and $\mu_L = 58$ nm, a much better fit of the signal is obtained.

The resulting distribution is compared with AFM measurements in figure 5. If the frequency function obtained by counting 70 particles is parametrized by a log-normal

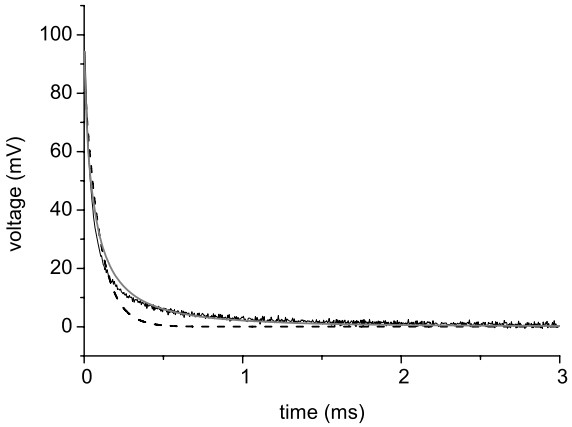


**Figure 4.** Relaxation signal for the fractionated (0.5 A) ferrofluid (black line) and results for the exponential fit (dashed line) and the fit using the log-normal distribution (grey line).

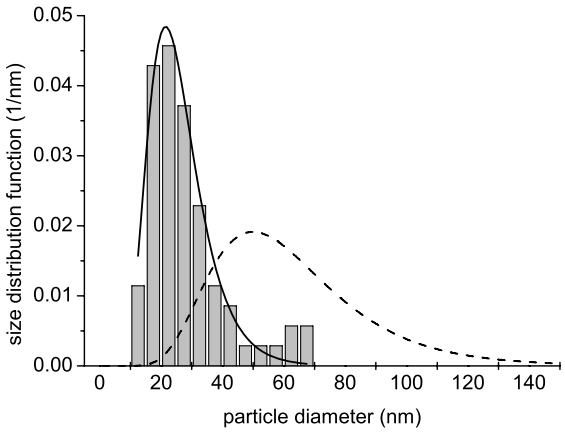


**Figure 5.** Size distribution function of the fractionated (0.5 A) ferrofluid obtained by AFM (grey bars, continuous line) and MORFF (dashed line) measurements. The parameters of the log-normal distribution are: AFM—$\mu_L = 24$ nm, $\sigma_L = 0.36$, MORFF—$\mu_L = 58$ nm, $\sigma_L = 0.39$.

distribution, too, the calculated shape parameter $\sigma$ is similar. However, the centre of the distribution determined by MORFF is shifted to higher values of the particle diameter.

### *3.2. Observation of biological binding reactions*

After each streptavidin functionalization of the MNP in preparation of the antibody attachment the streptavidin–MNP were reviewed in order to check their binding capacity. The addition of biotinylated bovine serum albumin (BSA-biotin) in different amounts yielded an increase in the particle sizes as described previously [13].

Binding experiments with the model systems hIgG/anti-hIgG are shown in figure 6. The addition of hIgG to anti-hIgG–MNP yielded an increase in the particle size in any case after 2 and 6 h of incubation (figure 6). Within the 6 h of incubation 1 $\mu$g hIgG effectuated a maximum change in particle sizes of 26%. The control incubation with hIgM showed only a slight increase. A similar result could be achieved within the hIgM/anti-hIgM system (data not shown).

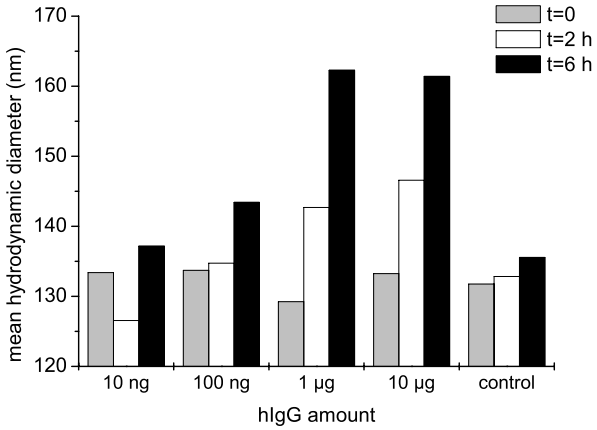


**Figure 6.** Mean hydrodynamic diameter from exponential fit from the incubation of anti-hIgG–MNP and hIgG at 0, 2 and 6 h. Control: 1 $\mu$g hIgM.

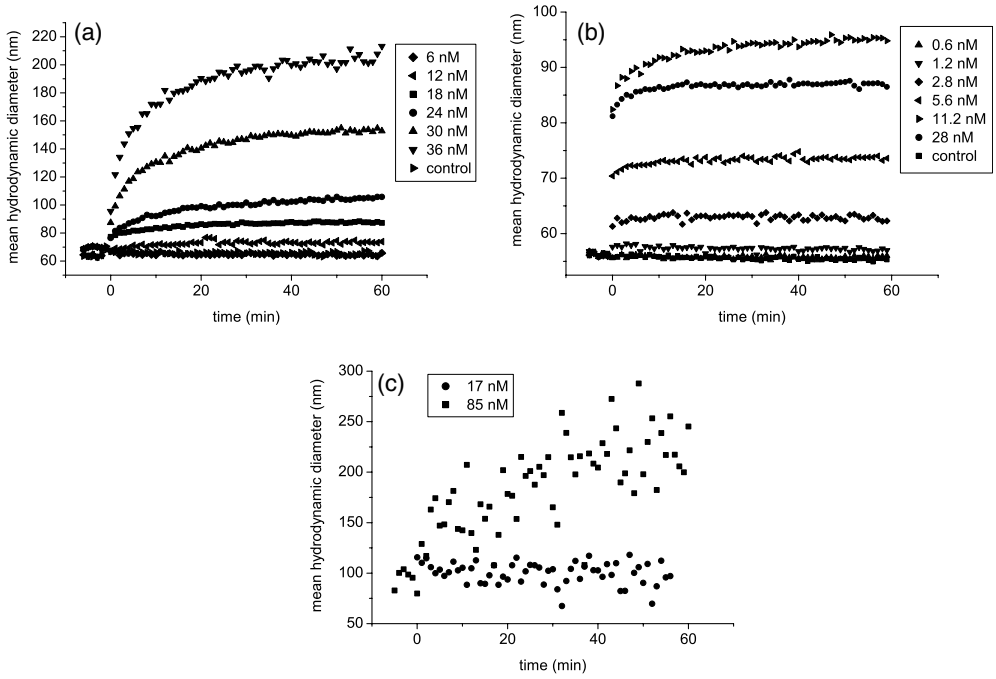


**Figure 7.** Mean hydrodynamic diameter obtained by an exponential fit from the incubation of anti-hEotaxin–MNP with hEotaxin (a), anti-hCEA–MNP with hCEA (b), and anti-hInsulin–MNP and hInsulin (c). Control: 3 nM bovine serum albumin (BSA).

The successful investigation of the model systems resulted in binding experiments with clinical relevant systems. Up to the present the properties of hEotaxin, hCEA, and hInsulin and their polyclonal antibodies were analysed by MORFF. After the attachment of the antibodies onto the streptavidin–MNP the incubation with the adequate antigen caused increasing hydrodynamic diameters (figure 7). Within 60 min the particle size of anti-hEotaxin–

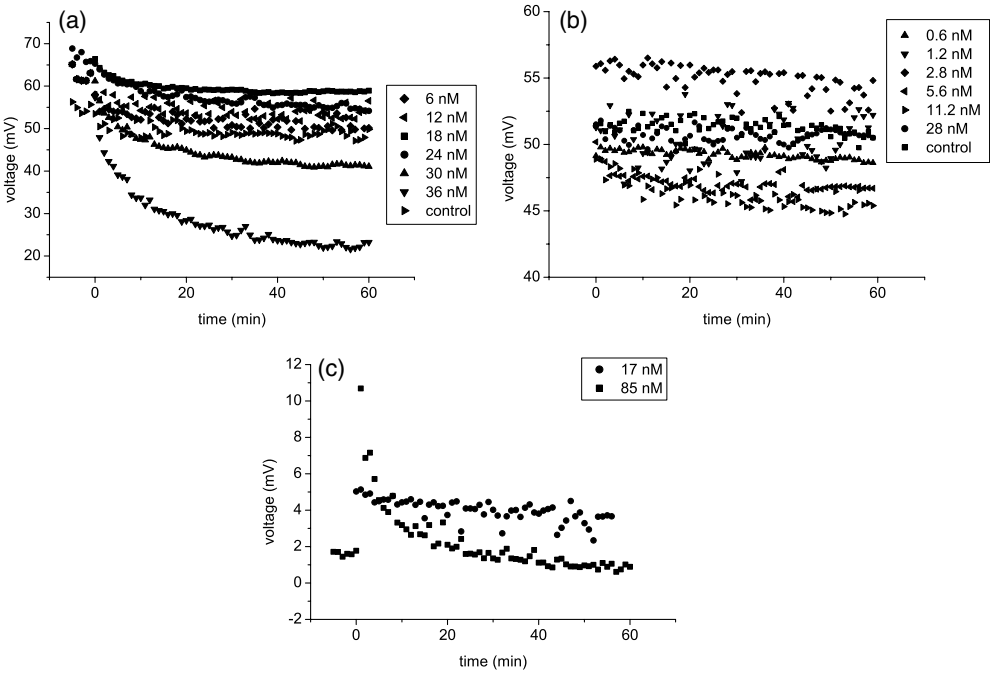


**Figure 8.** Amplitudes of the interactions of anti-hEotaxin–MNP and hEotaxin (a), anti-hCEA–MNP and hCEA (b), and anti-hInsulin–MNP and hInsulin (c) illustrated as voltage versus time. Control: 3 nM bovine serum albumin (BSA).

MNP ascended up to 300% due to the addition of 36 nM hEotaxin (figure 7(a)). Steady state conditions occurred after almost 30 min. Considering the hCEA/anti-hCEA system an incubation of the anti-hCEA–MNP with 1.2 nM and higher amounts of hCEA caused an increasing diameter. Nevertheless, it is remarkable that the diameter of the anti-hCEA–MNP shows a higher increase (up to 180%) when incubating with 11.2 nM hCEA as with 28 nM hCEA. Steady state was already achieved after 5–10 min in any case (figure 7(b)). However, hInsulin and its antibody show a completely different way of interaction (figure 7(c)). Only the application of one antigen concentration (85 nM) yielded an increase in the particles' diameter. Steady state conditions could not be reached within 60 min. Moreover, scattering of the particle size can be observed in contrast to the above described systems representing low noise curves.

Control experiments were performed for all systems by incubating the antibody–MNP with 3 nM BSA. In this case, the particle size persists at the initial diameter.

The amplitude of the static birefringence signal $I_0$ is shown in figure 8 as a function of reaction time for the three analysed systems. Preparing anti-hEotaxin–MNP and 6–24 nM hEotaxin yielded only a slight reduction in amplitude values. Indeed the amplitude of the 30 nM decreased by 35%, whereas the largest decrease of the amplitude value can be observed after the addition of 36 nM hEotaxin (figure 8(a)). Addition of hCEA solutions to the anti-CEA–MNP entailed nearly no reduction in the amplitude values (figure 8(b)). Merely the addition of the 11.2 nM antigen caused a slight decay of the amplitude curve. However, since the above mentioned amplitude values reached approximately 50 mV the analysis of the amplitudes of the hInsulin/anti-hInsulin system resulted in values of only 5 mV. The solution of 17 nM hInsulin produced no amplitude change, 85 nM lowered the amplitude up to nearly 2 mV.

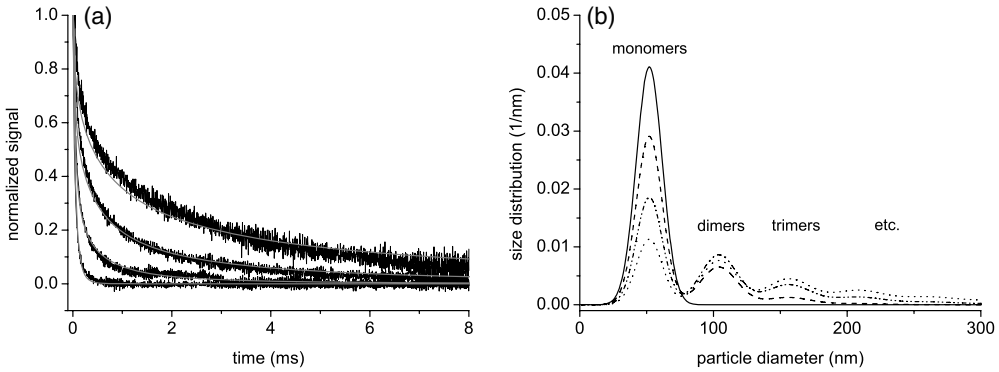


**Figure 9.** (a) Relaxation signals of the incubation of anti-hEotaxin–MNP with 36 nM hEotaxin at 0, 0.5, 3.5, and 60 min (bottom to top line) incubation time fitted by means of the chain model (grey lines); (b) resulting aggregate distribution at 0 min (continuous line), 0.5 min (dashed line), 3.5 min (chain dotted line) and 60 min (dotted line).

### *3.3. Analysing binding kinetics*

First, the parameters of the Gaussian distribution were optimized with respect of the initial relaxation signal, which was obtained before starting the coupling reaction. The result represents the size distribution of the MNP monomers in our model. For the MNP fraction used in our coupling experiments with hEotaxin, we obtain $\mu = 50.5$ nm, $\sigma = 10.9$ nm. The systematic increase of the relaxation time detected after the addition of antigen is demonstrated in figure 9(a). Applying our model for the formation of linear chains, the parameter $\alpha$ describing the conversion of antigen molecules was calculated fitting the intensity given by the equations (5) and (14) to the experimental relaxation signal. During the reaction of anti-hEotaxin–MNP with 24 nM hEotaxin, the parameter increases up to a value $\alpha = 0.5$ representing a conversion rate of antigen epitopes up to 70%. An increasing fraction of MNP aggregates, such as dimers, trimers etc, is reflected by the respective changes of the calculated size distribution, see figure 9(b).

The expectation value of the chain distribution, given by $\bar{d} = \mu(1 + \alpha)/(1 - \alpha)$ can be compared to the hydrodynamic diameter obtained from a monoexponential fit according to equation (4). In our calculations, both parameters deviate less than 15% for all investigated binding systems. In figure 10, the normalized expectation values are shown as a function of time for different antigen amounts. To obtain information about the rate constants of the elementary binding process between antigen and antibody, the kinetic equation (16) was solved for every antigen concentration, and the parameters $k_a$ and $k_d$ were determined by fitting the conversion to the values obtained via the distribution function. For hEotaxin, the results for $K_D = k_d/k_a$ vary from $K_D = 100$ nM at low antigen concentration to $K_D = 11$ nM for 36 nM hEotaxin.

For hCEA, values found for $K_D$ show the same systematic decrease with increasing antigen concentration, and the order of magnitude for $K_D$ is comparable (no figure shown). However, the time needed for steady state conditions, where no further change of the particles' diameter could be detected, is much shorter than for hEotaxin. This is reflected by an association rate constant of $k_a \approx 5 \times 10^7$ l mol$^{-1}$ min$^{-1}$, about ten times larger than the value obtained for hEotaxin. Because of the relatively poor quality of the data for hInsulin, a kinetic analysis was not performed for this system.

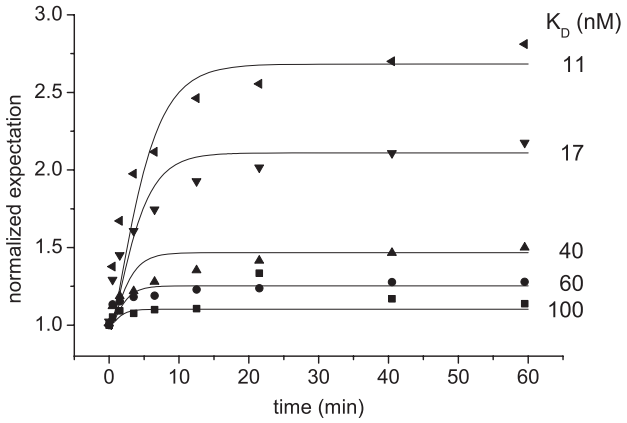


**Figure 10.** Normalized expectation value $\bar{d}/\mu = (1+\alpha)/(1-\alpha)$ of the incubation of anti-hEotaxin–MNP with 12, 18, 24, 30 nM and 36 nM hEotaxin (bottom to top line). Curves were fitted by the kinetic equation (16) for the derivation of $K_D$.

### *3.4. SPR*

For kinetic experiments using SPR it is vital to keep the maximal binding capacity ($R_{max}$) low and the flow rate high enough in order to avoid mass transport effects, crowding and aggregation [21]. Thus, antibodies were immobilized so that an $R_{max}$ of 50–100 RU could be achieved and binding experiments were performed at flow rates $\geqslant 30\ \mu l\ min^{-1}$. We applied different flow rates for each system since steady state conditions could only be reached in this manner due to different affinities of the antibody/antigen systems.

In figures 11(a)–(c) results of the three binding experiments are depicted in overlay plots of the different antigen concentrations as response units over time. The injection of hEotaxin (1–100 nM) over an anti-hEotaxin loaded surface results in an increase in response units in either case (figure 11(a)). Equilibrium could be reached with the addition of 5 nM and higher concentrations of hEotaxin. An abrupt rise in the association curve is followed by a more planar part as observed in almost the same manner in the dissociation phase. In contrast, the analysis of the hCEA/anti-hCEA system reveals a less rapid association and dissociation phase (figure 11(b)). Steady state conditions could hardly be reached. Only the addition of the highest concentration of hCEA (500 nM) ensued equilibrium. Passing hInsulin in a concentration range from 0.2 to 5.0 $\mu$M over the anti-hInsulin loaded flow cell yields a faster increase in response units as with the systems mentioned above (figure 11(c)). Within each concentration equilibrium is achieved. However, a maximum binding capacity of only 21 RU indicates a weak bond between hInsulin and its antibody.

The curves of each sensogram were fitted globally with a 1:1 (Langmuir) fit function integrated in the BIAevaluation software resulting in rather poor fits with all three system. Thereby the smallest equilibrium constant of 0.7 nM was obtained for the hEotaxin/anti-hEotaxin system. hCEA and its antibody produced a $K_D$ one order of magnitude larger of 37.2 nM. For the hInsulin/anti-hInsulin system a $K_D$ of 522 nM was found.

## 4. Discussion and conclusion

This study combines the characterization of ferrofluids, the qualitative detection of biomolecular binding reactions and the determination of kinetic properties of different

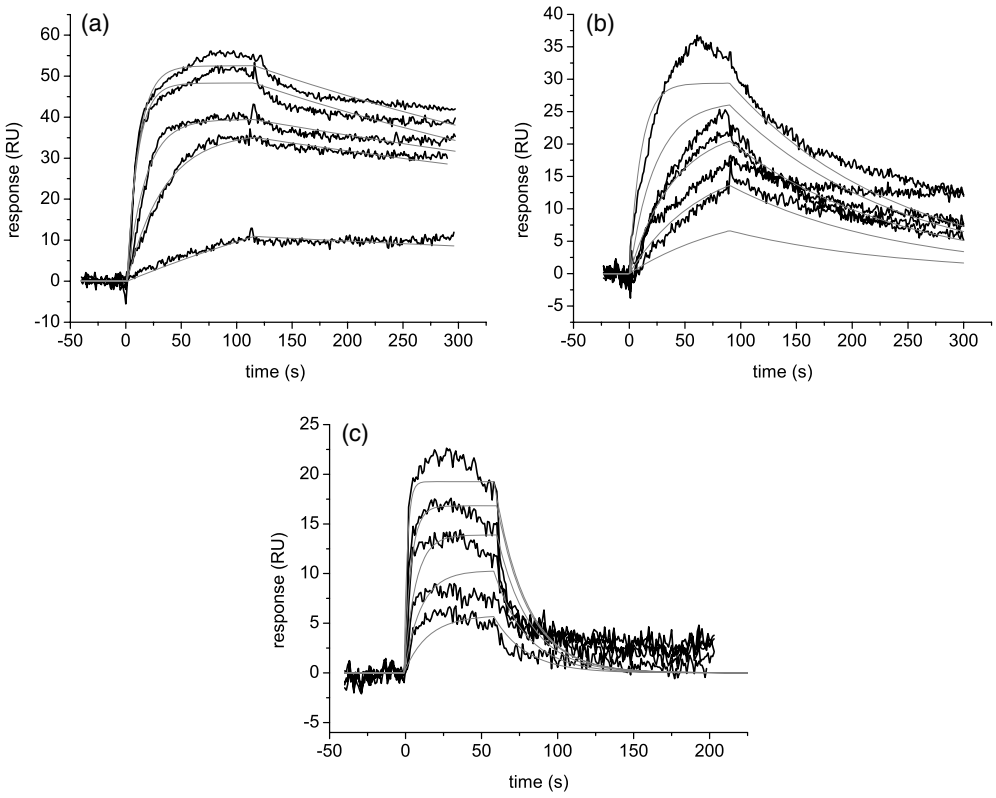


**Figure 11.** Sensograms of immobilized anti-hEotaxin binding hEotaxin ((a); 1, 5, 10, 50, 100 nM, bottom to top line), anti-hCEA binding hCEA ((b); 20, 50, 100, 200, 500 nM, bottom to top line), anti-hInsulin binding hInsulin ((c); 0.2, 0.5, 1, 2, 5 $\mu$M, bottom to top line), plotted as the mass of protein binding (RU) to immobilized antibodies as a function of time. Experimentally derived curves (black lines) from twice repeated injections of the antigens at various concentrations are shown overlaid. Curves were fitted globally with BIAevaluation 4.1 software using a 1:1 (Langmuir) fit (grey lines).

antibody/antigen systems by means of measurements of the magneto-optical birefringence of functionalized MNP. For this purpose a table-top device was developed utilizing the Cotton–Mouton effect. By virtue of separation of optical detection from magnetic stimulation, measurements could be performed without extensive magnetic shielding as required in magnetic relaxation measurements [3]. Functionalization of MNP was accomplished using standard reagents and procedures. Binding experiments were started by adding antigen to a cuvette with 1 ml functionalized MNP suspension. In this work we were able to detect the interactions even of small proteins like the proteinogenic hormone hInsulin (5.8 kDa), and the chemokine hEotaxin (8.4 kDa) with their antibodies. Further on, MORFF exhibits currently a limit of detection (LOD) in the pM range (hIgG/anti-hIgG) and nM range (hCEA/anti-hCEA). In this respect it is comparable to similar methods [22].

The magnetic properties as well as shape and size distribution of the MNP are of great relevance for the detection principle. No optical birefringence results from very small nanoparticles, because Néel relaxation [23] yields an alignment of the magnetic moments inside the particles along the external field without rotation of the entire particles. Magnetic fractionation was performed to minimize signal loss due to Néel relaxation. However,

the size distribution of the obtained larger nanoparticles is still broad, as indicated by the nonexponential relaxation of the MNP and by the AFM measurement. The preparation of particles with a narrow size distribution, blocked Néel relaxation and strong shape anisotropy could lead to a further increase of the signal strength and sensitivity.

It was demonstrated that MORFF is applicable for size measurements. The hydrodynamic diameters of MNP fractions obtained by MORFF are smaller than the respective values of PCS measurements. For Rayleigh scattering, which is relevant for particles much smaller than the wavelength of the light, the intensity of the scattered light is proportional to the 6th power of the particle diameter. This could yield a strong weighting of the larger particles of the size distribution resulting in larger effective diameters obtained by PCS. Our AFM measurements confirm the shape parameter $\sigma$ of the log-normal distribution obtained by MORFF. However, the value of the centre of the function is much smaller because AFM is performed with particles adsorbed on mica in air yielding collapsed particle shells.

This study succeeded in coupling proteins with the MNP via the periodate method and the following streptavidin–biotin binding system. hIgG and hIgM and their respective antibodies acted as model systems. The addition of increasing amounts of antigen to the antibody coupled MNP yielded an accretion of the particles until an optimum in the antibody/antigen ratio was reached. After this optimum the particle size increases to a lesser extent (see figure 6). In particular, the interaction of the hCEA/anti-hCEA system exhibits this behaviour. An addition of 28 nM antigen caused a slighter aggregate size than the addition of 11.2 nM (figure 7(b)). This is in good agreement with Heidelberger *et al* [24] who demonstrated that when an increasing amount of an antigen is added to a constant amount of corresponding antibody, the resulting degree of precipitate formed follows a bell shaped curve.

Regarding the signal amplitudes as a function of antigen concentration may contain further information. In the hEotaxin/anti-hEotaxin system amplitudes follow a systematic behaviour, whereby the addition of the highest antigen concentration causes a maximum decrease in amplitude values. This phenomenon may be caused by the formation of large aggregates, which have lost their anisotropy and thus the capability to align in the magnetic field.

For anti-hInsulin loaded MNP, we detect particle aggregation already before the antigen addition. The *in vitro* aggregation of wild-type proteins, such as a polyclonal antibody, is affected by the local environment [25]. The pH, the presence and concentration of ions and particularly the particle surface properties play an important role in this case and may cause antibody aggregation without any antigen.

Within our model of stepwise polymerization, the prolongation of the relaxation time can be explained by a distribution function, which includes monomers as well as dimers, trimers etc. The optimization of the conversion parameter $\alpha$ leads to a reasonable agreement of the modelled curve with the relaxation signal, even for the slowest relaxations obtained in our coupling experiments. The simple exponential fit does not fully meet the relaxation signal; however, we could demonstrate that the diameter derived from the exponential fit is well comparable with the expectation value of the broad size distribution function. Therefore, if no detailed information about the size distribution of the MNP and their aggregates are needed, the conversion of binding sites can be calculated from the normalized diameter $d_{\mathrm{norm}} = d_{\mathrm{hyd}}/d_{\mathrm{hyd},0}$ as $\alpha = (d_{\mathrm{norm}} - 1)/(d_{\mathrm{norm}} + 1)$. The conversions calculated for hEotaxin for different amounts of antigen cannot be described by a single $K_{\mathrm{D}}$. The broad range of values obtained for equilibrium constant can be partially explained by the polyclonality of the system. Furthermore, cross-linking between chain sections may yield to more stable aggregates at high antigen concentrations.

It has to be mentioned that the modelling of the effective size of the MNP aggregates is of great relevance. Using relation (13), we assumed the addition of the diameters, i.e. a

dimer has double the size of a monomer. For the relaxation time of the aggregates follows $\tau_N = \tau \times n^3$. Alternatively, the relaxation behaviour of an $n$-mer can be described as similar to a sphere with the same volume, yielding $\tau_N = \tau \times n$ [26]. For the latter assumption, a higher degree of polymerization follows from the fit of a relaxation signal. The resulting $K_D$ values can be smaller up to two orders of magnitude. In the calculations presented here, we used the first model of additive diameters, because the broader distribution function does better fit the relaxation signal. For a deeper understanding of the size distribution, additional measurements are required as from magnetic fractionation of aggregates or size exchange chromatography.

For the three antibody/antigen systems with clinical relevance SPR measurements were conducted (figure 11). The hEotaxin/anti-hEotaxin chart reveals an obvious division of the association curve into at least two parts, a rapid part within the first 30 s and a slower one within the residual 90 s (figure 11(a)). This suggests the presence of a heterogeneous ligand as it is represented by a polyclonal antibody. A high signal to noise ratio has to be anticipated for the curves of the hInsulin/anti-hInsulin curves, due to the small antigen (5.8 kDa) having not the ability to cause large effects.

The obtained response curves of all three systems were fitted globally by a 1:1 (Langmuir) fit assuming homogeneous binding partners. Fitting the curve progressions yielded a poor fit in any case. Since the ligand is a polyclonal antibody consisting of a blend of antibodies recognizing different antigen epitopes only the avidity of the system could be determined. The avidity is, in contrast to the affinity, the bond strength of a multivalent antigen and a multivalent antibody. In order to receive uniform parameters as from the MORFF measurements we decided to apply the 1:1 (Langmuir) fit. The determined values for the equilibrium constants are well comparable with results determined by Kure *et al* [27] (hInsulin), Seet *et al* [28] (hEotaxin), and Garambois *et al* [29] (hCEA). In contrast, the kinetic parameters obtained by SPR do not support the results of our MORFF measurements. A different behaviour of an antibody/antigen system is depicted with both measurement methods.

In conclusion, MORFF size measurements give comparable results to other methods, and the modelled distribution functions including aggregates are able to describe the shape of the relaxation signal during coupling reactions between antigen and antibody. For a quantitative description of the basic kinetic processes yielding rate constants a deeper insight into the relaxation behaviour of aggregate structures is needed. Experiments using monoclonal antibodies are in preparation which should enable a more definite kinetic description.

## Acknowledgments

We thank Manesh Gopinadhan for assistance with AFM measurements, and Elena Heister and Franziska Aswaldt for excellent technical assistance. The support of this research project by the German Research Foundation under contract no. WE2555/1 is gratefully acknowledged.

## References

[1] Pankhurst Q A, Connolly J, Jones S K and Dobson J 2003 *J. Phys. D: Appl. Phys.* **36** R167–81
[2] Haik Y, Pai V and Chen C-J 1999 *J. Magn. Magn. Mater.* **194** 254–61
[3] Weitschies W, Kötitz R, Bunte T and Trahms L 1997 *Pharm. Pharmacol. Lett.* **7** 5–8
[4] Chemla Y R, Grossman H L, Poon Y, McDermott R, Stevens R, Alper M D and Clarke J 2000 *Proc. Natl Acad. Sci. USA* **97** 14268–72
[5] Büscher K, Helm C A, Gross C, Glöckl G, Romanus E and Weitschies W 2004 *Langmuir* **20** 2435–44
[6] Cotton A and Mouton H 1907 *C. R. Hebd. Seances Acad. Sci.* **145** 229–30
[7] Luster A D and Rothenberg M E 1997 *J. Leukoc. Biol.* **62** 620–33
[8] Yu Y, Sweeney M D, Saad O M, Crown S E, Handel T M and Leary J A 2005 *J. Biol. Chem.* **280** 32200–8

[9] Baggiolini M, Dewald B and Moser B 1997 *Annu. Rev. Immunol.* **15** 675–705
[10] Chester K A *et al* 2000 *Cancer Chemother. Pharmacol.* **46** (Suppl.) S8–12
[11] Yalow R S and Berson S A 1959 *Nature* **184** (Suppl. 21) 1648–9
[12] Andersen L, Dinesen B, Jorgensen P N, Poulsen F and Roder M E 1993 *Clin. Chem.* **39** 578–82
[13] Romanus E, Gross C, Kötitz R, Prass S, Lange J, Weber P and Weitschies W 2000 *Magnetohydrodynamics* **2** 328–33
[14] Fannin P C, Kinsella L and Charles S W 1999 *J. Magn. Magn. Mater.* **201** 91–4
[15] Perrin F 1934 *J. Phys. Radium* **5** 497–511
[16] Romanus E, Gross C, Glöckl G, Weber P and Weitschies W 2002 *J. Magn. Magn. Mater.* **252** 384–6
[17] Ferre J and Gehring G A 1984 *Rep. Prog. Phys.* **47** 513–611
[18] Dotson N A, Galvan R, Laurence R L and Tirrell M 1996 *Polymerization Process Modeling* (New York: VCH Publishers)
[19] O'Shannessy D J, Brigham-Burke M, Soneson K K, Hensley P and Brooks I 1993 *Anal. Biochem.* **212** 457–68
[20] Andersson K, Hamalainen M and Malmqvist M 1999 *Anal. Chem.* **71** 2475–81
[21] Myszka D G, Morton T A, Doyle M L and Chaiken I M 1997 *Biophys. Chem.* **64** 127–37
[22] Seydack M 2005 *Biosens. Bioelectron.* **20** 2454–69
[23] Néel L 1949 *Ann. Geophys.* **5** 99–136
[24] Heidelberger M and Kendall F E 1935 *J. Exp. Med.* **62** 697–720
[25] Demeule B, Gurny R and Arvinte T 2006 *Eur. J. Pharm. Biopharm.* **62** 121–30
[26] Aurich K, Nagel S, Glöckl G and Weitschies W 2006 submitted
[27] Kure M, Katsura Y, Kosano H, Noritake M, Watanabe T, Iwaki Y, Nishigori H and Matsuoka T 2005 *Intern. Med.* **44** 100–6
[28] Seet B T, McCaughan C A, Handel T M, Mercer A, Brunetti C, McFadden G and Fleming S B 2003 *Proc. Natl Acad Sci. USA* **100** 15137–42
[29] Garambois V, Glaussel F, Foulquier E, Ychou M, Pugniere M, Luo R X, Bezabeh B and Pelegrin A 2004 *BMC Cancer* **4** 75